Pure and Applied Functional Analysis
Volume 4, Number 4, 2019, 825–848

Yokohama Publishers
ISSN 2189-3764 ONLINE JOURNAL

TOPOLOGY DESIGN OF THERMOMECHANICAL ACTUATORS COMBINED WITH HEAT SOURCE OPTIMIZATION

S. M. GIUSTI, Z. MRÓZ, A. A. NOVOTNY, AND J. SOKOŁOWSKI

Abstract. In the paper a problem of optimal topology and shape design of thermo-mechanical actuators with the heat source support is considered. The objective is to maximize the output displacement in a prescribed direction on the actuator boundary interacting with an external elastic support exerting localized reaction force. The thermal excitation results from the heat sources applied within the body domain and the thermal boundary conditions. This action induces the volumetric thermal strain field and the residual stress field within the actuator domain. The problem is modeled by a semi-coupled system of differential equations, where the mechanical field is governed by the Navier equation of the plane stress elasticity, coupled with the steady state heat conduction problem governed by the Poisson equation. Several solved specific cases illustrate the design evolution depending on the ratio of support and averaged actuator stiffness.

1. Introduction

In the paper the topology design of thermomechanical actuators is considered for linear multiphysics model in the structure of reference configuration given by an open and bounded domain $\Omega \subset \mathbb{R}^2$, with Lipschitz boundary denoted as $\partial\Omega$. The displacement field is determined within linear elasticity with thermally induced stresses. The temperature field is described by the steady-state heat conduction equation. The state variables include the displacement field u and the temperature field θ. The shape functional $J(\Omega)$ to be minimized is given by the integral of the quantity $g = -u \cdot e$ on $\Gamma^\star$. So that the idea is to maximize the output displacement u in a given direction e on a part of the boundary $\Gamma^\star \subset \partial\Omega$, interacting with the external body simulated by an elastic support exerting the reaction force.

For the purposes of optimum design we are interested in locations and sizes of finite number of inclusions in Ω. For the sake of simplicity, the sensitivity analysis $\Omega \mapsto J(\Omega)$ is performed for a single inclusion $\varepsilon \mapsto B_\varepsilon(\widehat{x})$ with the fixed center $\widehat{x} \in \Omega$, where B_ε is a ball of radius ε. As a result, the asymptotic expansion of $J(\Omega)$ with respect to small parameter ε is established at $\varepsilon = 0^+$. The result of sensitivity analysis is called the topological derivative and it depends on the solutions u and θ, as well as on their corresponding adjoint states, all of them evaluated at the center

2010 *Mathematics Subject Classification.* 47N10, 49N05, 65K10 and 90C31.
Key words and phrases. topological derivative, thermomechanical actuators, topology and shape variations, optimum design.

$\widehat{x}$, on the material parameters for mechanical and thermal properties, and on the intensity of the heat source.

For the sake of simplicity the unique contrast $0 < \gamma < \infty$ for the coefficients of elliptic operators is introduced, which means that the material parameters for mechanical and thermal properties of the small inclusion B_ε are governed by the scalar γ. This assumption can be relaxed for the specific applications, if necessary. In addition we introduce the contrast $0 < \gamma^b \leq 1$ for the intensity of the heat source.

In this way an optimal location of small inclusion and its properties can be determined in order to minimize the shape functional associated with the model. The topological derivative of the elastic energy associated with such thermomechanical model has been derived in [9]. However, to our best knowledge the topological sensitivity analysis of a shape functional specially designed for topology optimization purposes of thermomechanical actuators cannot be found in the literature. Therefore, we derive in all details the topological asymptotic expansion of the adopted shape functional and perform a complete mathematical justification for the obtained formulas.

In the paper we consider the regular perturbations of the coefficients of elliptic operators as well as of the right hand side for the purposes of asymptotic analysis. The case of singular perturbations can be considered as well [17] along the lines of the fundamental paper [16]. Self-adjoint extensions of elliptic operators can be used to model defects for control problems, we refer the reader to [12] for some results in this direction. Control problems for the wave equations [13] are considered in [14] from the point of view of sensitivity analysis.

The paper is organized as follows. In Section 1.1 a simple example of a two-bar structure is presented to illustrate the design evolution dependent on the stiffness ratio of the interacting spring and bar. In Section 1.2 the topological derivative concept is introduced in the framework of asymptotic analysis of singulary perturbed domain. The semi-coupled system modeling the thermomechanical actuator as well as the adopted shape functional are presented in Section 2. The topological optimization procedure is introduced in details in Section 3. In Section 4 some numerical experiments of topology optimization of thermomechanical actuators are presented. Finally, the concluding remarks and perspectives are given in Section 5.

1.1. **Motivation: a simple example.** As a motivation for this work, let us introduce a simple analytical example on the optimal design of a thermomechanical actuator. Consider a two-bar system with hinge supports at two points A and C; and a hinge at a joint point B, see Fig. 1. At the connection point B the bars are interacting with the rigidly supported spring of stiffness k_s.

By heating the bars, the vertical displacement at point B is activated and the induced spring force $P = k_s(h - h_0)$ generates compressive force $T = \frac{P}{2\sin\beta}$ in the bars. Assume the cross-section area A_r and the total length of bars to be fixed. The optimal configuration of the bars specified by the angle β is to be determined, such that the incremental displacement dh of the point B is maximized. Denoting by θ the temperature and by α the thermal expansion coefficient, the optimization

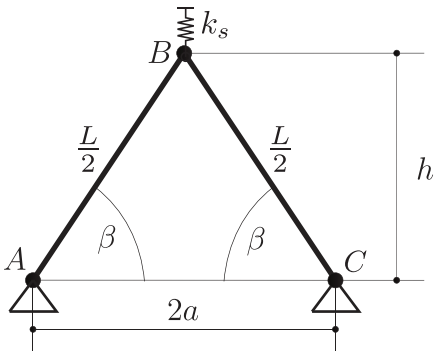

FIGURE 1. Two bars truss submitted to thermal effects.

problem can be stated as follows:

$$\begin{cases} \underset{\beta}{\text{Maximize}} & \mathcal{F}(\beta) &= \frac{dh}{\alpha \frac{L}{2} d\theta}, \\ \text{Subjected to} & L &= constant, \end{cases} \tag{1.1}$$

Following Fig. 1, we have $a = \frac{L}{2}\cos\beta$ and $h = \frac{L}{2}\sin\beta$. Therefore, the differential elements da and dh are given by

$$da = -\tfrac{L}{2}\sin\beta d\beta + \tfrac{dL}{2}\cos\beta, \tag{1.2}$$

$$dh = \tfrac{L}{2}\cos\beta d\beta + \tfrac{dL}{2}\sin\beta. \tag{1.3}$$

To consider the restriction of the total length of the bars L must be constant, we can set in (1.3) $da = 0$ and obtain the following relations

$$d\beta = \frac{dL}{L}\cot\beta\,, \quad \text{and} \quad dh = \frac{dL}{2\sin\beta}\,. \tag{1.4}$$

The spring force increment $dP = k_s dh$ induces a compressive bar force increment $dT = \frac{dP}{2\sin\beta}$ and the related strain increment $d\epsilon$ is

$$d\epsilon = -\frac{dP}{2\sin\beta}\frac{1}{EA_r} = -\frac{k_s dh}{2\sin\beta}\frac{1}{EA_r}\,, \tag{1.5}$$

where E is the Young's modulus of the material. The total bar elongation now equals

$$dL = \frac{L}{2}\left(\alpha d\theta - \frac{k_s dh}{2\sin\beta}\frac{1}{EA_r}\right) = 2\sin\beta dh\,. \tag{1.6}$$

Therefore, from equations (1.1) and (1.6) it follows that

$$\mathcal{F}(\beta) = \frac{1}{2\sin\beta + \frac{\eta}{4\sin\beta}} = \frac{1}{D}\,, \tag{1.7}$$

where $\eta = \frac{k_s}{EA_r/L}$ is the ratio of the spring and bar stiffness. This is a fundamental parameter of the structure response. It is seen that $\mathcal{F}(\beta)$ reaches its maximum when the denominator D reaches a minimum, thus

$$\frac{dD}{d\beta} = \frac{\cos\beta}{4}\left(8 - \frac{\eta}{\sin^2\beta}\right) = 0\,, \tag{1.8}$$

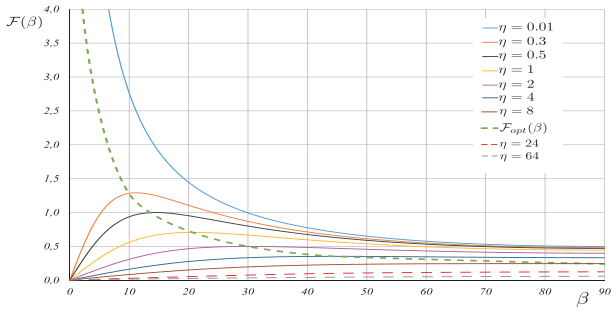

FIGURE 2. Behaviour of the function $\mathcal{F}(\beta)$.

and the optimal configuration is specified for β satisfying the condition:

$$\sin\beta = \sqrt{\frac{\eta}{8}} = \frac{1}{2}\sqrt{\frac{\eta}{2}}\,, \quad \Rightarrow \quad \eta \leq 8 \quad \text{and} \quad \mathcal{F}_{opt}(\beta) = \frac{1}{\sqrt{2\eta}} \tag{1.9}$$

For $\cos\beta = 0$, its follows that $\beta = \frac{\pi}{2}$ and $a = 0$ and the configuration corresponding to two vertical bars, attains a local maximum of $\mathcal{F}(\beta)$. For $\eta = 0$, from (1.9) it follows that the optimal configuration is at $\beta = 0$ and $a = \frac{L}{2}$. It is represented by two coaxial bars. This case was discussed in the paper [6]. For values of $\eta > 8$, eq.(1.8) is satisfied only for $\beta = \frac{\pi}{2}$. Figure 2 presents the dependence of $\mathcal{F}(\beta)$ on β and η, and the optimal configurations depending on η are drawn in a dashed line. For instance, in Figure 3 the optimal configurations for three values of the parameter η are presented. Note that the optimal configuration of the truss does not depend on the value of the temperature θ and the thermal expansion coefficient α.

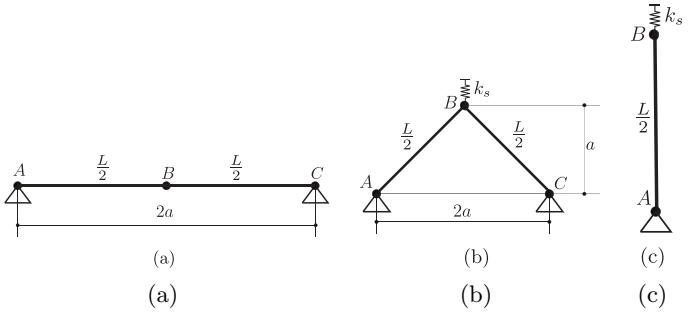

(a) (b) (c)

FIGURE 3. Optimal configurations for (a) $\eta = 0$, (b) $\eta = 4$ and (c) $\eta > 8$.

The present example illustrates the evolution of optimal design configuration depending on the stiffness ratio . For the actuator not interacting with an external body, the values $\eta = 0$ and $\beta = 0$ indicate the design, for which the maximal element rotation and the presence of rotational hinges are required in the continuum to promote the maximal deflection by the initial strain field. This case was analyzed in the previous paper [6]. On the other hand, for increasing stiffness ratio η the effect of the reaction force increases, requiring the stress carrying members oriented

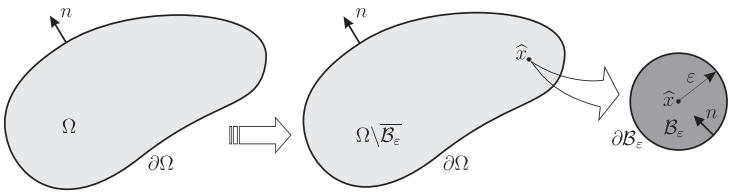

FIGURE 4. Topological derivative concept.

along the principal stress equilibrating the acting force, so the limiting configuration tends to $\beta = \frac{\pi}{2}$ for $\eta \geq 8$, thus resembling the familiar Michell structures composed of bars carrying compressive or tensile forces.

1.2. **Topological derivative concept.** The model of coupled equations which we are dealing with is linear elliptic, hence it is well posed from the point of view of shape optimization. For numerical solution of optimum design problems it is required to insert inclusions with different properties such as constitutive or heat source, the new properties are characterized by contrast parameters. For numerical solution of optimum design problems it is required to insert inclusions made from different material, the new material is characterized by two contrast parameters for elastic and thermal properties. The starting point of the numerical procedure of structural optimum design is the evaluation of the topological derivatives for the specific shape functionals which are taken into account for the optimization of the structure. The robust formulas for the topological derivatives are important since the precision of numerical evaluation of the formulas should be sufficient for the identification of local minima or maxima of the derivatives.

In order to introduce these concepts, let us consider an open bounded domain $\Omega \subset \mathbb{R}^2$, which is subjected to a non-smooth perturbation in a small region $\mathcal{B}_\varepsilon(\widehat{x})$ of size ε with center at an arbitrary point $\widehat{x} \in \Omega$. Thus, introducing a characteristic function $\chi = \mathbb{1}_\Omega$, associated to the unperturbed domain, it is possible to define the characteristic function associated to the topological perturbed domain χ_ε. Particularly, if the topological perturbation is a inclusion, we have $\chi_\varepsilon(\widehat{x}) = \mathbb{1}_\Omega - (1-\gamma)\mathbb{1}_{\overline{\mathcal{B}_\varepsilon(\widehat{x})}}$, where $\gamma \in \mathbb{R}^+$ is the contrast parameter, see Figure 4. Then it is assumed that a given shape functional $\psi(\chi_\varepsilon(\widehat{x}))$, associated to the topological perturbed domain, admits the following topological asymptotic expansion

$$\psi(\chi_\varepsilon(\widehat{x})) = \psi(\chi) + f(\varepsilon)\mathcal{T}_\chi(\widehat{x}) + o(f(\varepsilon)) \,, \tag{1.10}$$

where $\psi(\chi)$ is the shape functional associated to the unperturbed domain, $f(\varepsilon)$ is a function such that $f(\varepsilon) \to 0^+$, with $\varepsilon \to 0^+$. A function $\widehat{x} \mapsto \mathcal{T}_\chi(\widehat{x})$ is the so-called topological derivative of ψ in the point $\widehat{x}$. Thus, the topological derivative can be seen as a first order correction factor over $\psi(\chi)$ to approximate $\psi(\chi_\varepsilon(\widehat{x}))$. Note that, the shape functionals $\psi(\chi_\varepsilon(\widehat{x}))$ and $\psi(\chi)$ are associated to domains with different topologies. Therefore, the unknown function $\mathcal{T}_\chi(\widehat{x})$ it is determined by performing the topological asymptotic analysis (see, for instance, the book [17]).

In the following, we introduce the notation used in the paper for the contrasts, which characterize the topological perturbation of the constitutive parameters and heat source support. The continuous topological derivative is discretized for the

purposes of the gradient type a level set numerical method. The structure under considerations is defined in a subdomain Ω of the fixed hold all domain $\mathcal{D} \subset \mathbb{R}^2$. The characteristic function of Ω is denoted by χ. In the subdomain $\Sigma \subset \Omega$ the heating source is applied. The characteristic function of Σ is denoted by χ_b. Thus, within the numerical method the two characteristic functions are iterated in order to achieve the local optimality of combined design. For a general description, it is convenient to introduce two contrast functions γ and γ_b defined for our convenience in D, the functions uniquely determine the domains Ω and Σ. Namely,

$$\gamma(x) = \begin{cases} \rho_0 & \text{if} \quad x \in \Omega \\ \rho_1 & \text{if} \quad x \in \mathcal{D} \setminus \Omega\,, \end{cases}, \quad \text{and} \quad \gamma^b(x) = \begin{cases} \delta_0 & \text{if} \quad x \in \Sigma \\ \delta_1 & \text{if} \quad x \in D \setminus \Sigma\,, \end{cases} . \tag{1.11}$$

where $0 < \rho_0 << \rho_1$ and $0 < \delta_0 << \delta_1$. In our analyses, we select $\rho_0 << 1$, $\delta_0 << 1$, $\rho_1 := \rho_0^{-1}$ and $\delta_1 := \delta_0^{-1}$.

Remark 1.1. *It is clear that the asymptotic analysis with respect to the coefficients of the elliptic operator is involved. Such an analysis is simple in the case of the source.*

Remark 1.2. *It is convenient to consider the evolution of the domain Ω during the topological optimization in the whole hold all domain, that is why we can consider the extensions of the contrast functions to the hold all domain D.*

The topological derivative concept was rigorously introduced in [20]. Since then this concept has been widely used in several research areas and engineering applications, see for instance the works by [10, 11, 3, 8, 7, 21, 1] and the books [17, 18]. In particular, for the mathematical analysis related to the fully coupled piezoelectric problem see [5]. In particular, in this work, the topological derivative $\mathcal{T}_\chi(\widehat{x})$ will be used as a feasible descent direction in a computational framework for topology optimization.

2. Problem Formulation

Let us now introduce the thermomechanical semi-coupled model. Firstly, consider an open bounded domain $\mathcal{D} \in \mathbb{R}^2$, with smooth boundary $\partial\mathcal{D}$. Inside $\mathcal{D}$ is defined the domain Ω of the structural part, such that $\Omega \subseteq \mathcal{D}$. Then, $\mathcal{D}$ is the so-called *hold-all domain*. The displacement field in $\mathcal{D}$ is determined within the linear elasticity with thermally induced stresses for isotropic materials. The temperature field is described by the steady-state heat conduction equation. The state variables include the displacement field and the temperature field. The shape functional which we are dealing with is given by

$$\mathcal{J}(u) := -\int_{\Gamma^\star} e \cdot u\,, \tag{2.1}$$

where $\Gamma^\star$ is a part of the boundary $\partial\Omega$ where the displacement u has to be maximized in a given direction specified by the unit vector e. The vector function u solves the coupled system of boundary value problem, namely

$$u \in \mathcal{V}(\mathcal{D}) \;:\; \int_{\mathcal{D}} \sigma(u) \cdot (\nabla\xi)^s = \int_{\mathcal{D}} \rho\beta\theta \mathrm{div}(\xi) + \int_{\Gamma^\star} k_s u \cdot \xi \quad \forall \xi \in \mathcal{V}(\mathcal{D})\,. \tag{2.2}$$

The space of admissible displacements is defined as

$$\mathcal{V}(\mathcal{D}) := \left\{ \phi \in \mathbf{H}^1(\mathcal{D}) : \phi_{|\Gamma_u} = 0 \right\} , \tag{2.3}$$

with $\mathbf{H}^1(\mathcal{D}) := H^1(\mathcal{D}; \mathbb{R}^2)$ and Γ_u is used to denote a part of the boundary $\partial\Omega$ where the displacement u is prescribed. Also, in $\Gamma^\star$ is placed a spring with stiffness k_s. The parameter ρ in (2.2) is given by:

$$\rho = \left\{ \begin{array}{ccc} 1 & \text{in} & \Omega \\ \rho_0 & \text{in} & \mathcal{D} \setminus \Omega \end{array} \right. . \tag{2.4}$$

The Cauchy stress tensor related to the total displacement gradient is defined as

$$\sigma(u) := \rho \mathbb{C} (\nabla u)^s , \tag{2.5}$$

where $(\nabla u)^s$ is used to denote the symmetric part of the gradient of the displacement field u, i.e.

$$(\nabla u)^s := \frac{1}{2}(\nabla u + (\nabla u)^\top) . \tag{2.6}$$

In addition, $\mathbb{C}$ denotes the four-order elastic tensor given by

$$\mathbb{C} = 2\mu \mathbb{I} + \lambda (\mathrm{I} \otimes \mathrm{I}) , \tag{2.7}$$

where μ and λ are the Lame's coefficients. The coefficient β in (2.2) is defined as

$$\beta = \alpha(2\mu + 3\lambda) , \tag{2.8}$$

and α is the thermal expansion coefficient. In terms of Young's modulus E and Poisson ratio ν, there are

$$\mu = \frac{E}{2(1+\nu)}, \quad \lambda = \frac{\nu E}{(1+\nu)(1-2\nu)}. \tag{2.9}$$

For plane stress assumption λ and β must be replaced respectively by $\lambda^\star$ in (2.7) and $\beta^\star$ in (2.8), where

$$\lambda^\star = \frac{2\mu\lambda}{\lambda + 2\mu} = \frac{\nu E}{1-\nu^2}, \quad \beta^\star = 2\alpha(\mu + \lambda^\star). \tag{2.10}$$

Moreover, the scalar function θ in (2.2) is solution to the following boundary value problem

$$\theta \in \mathcal{H}(\mathcal{D}) \ : \ \int_{\mathcal{D}} q(\theta) \cdot \nabla \eta + \int_\Omega b_\delta \eta = 0 \quad \forall \eta \in H_0^1(\mathcal{D}) , \tag{2.11}$$

where b_δ is used to denotes a heat source applied in a region $\Sigma \subseteq \Omega$. For our convenience b_δ is extended to Ω by the small parameter δ_0:

$$b_\delta = \left\{ \begin{array}{ccc} 1 & \text{in} & \Sigma \\ \delta_0 & \text{in} & \Omega \setminus \Sigma \end{array} \right. . \tag{2.12}$$

See details of the coupled system in Fig. 5.

The set of admissible temperatures is defined as a cone in the Sobolev space

$$\mathcal{H}(\mathcal{D}) := \left\{ \phi \in H^1(\mathcal{D}) : \phi_{|\Gamma_\theta} = \overline{\theta} \right\} , \tag{2.13}$$

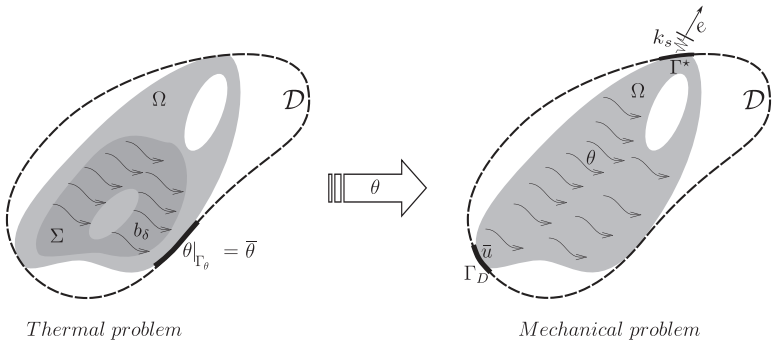

FIGURE 5. Thermo-mechanical semi-coupled problem.

with Γ_θ used to denote a part of the boundary $\partial\mathcal{D}$ where the temperature θ is prescribed by a given function $\overline{\theta}$. The heat flux vector is defined as

$$q(\theta) = -\rho \mathrm{K} \nabla\theta \,, \tag{2.14}$$

where K is a second order tensor representing the thermal conductivity of the medium. In the isotropic case, the tensor K can be written as

$$\mathrm{K} = k\mathrm{I} \,, \tag{2.15}$$

being k the thermal conductivity coefficient. Let us also introduce the adjoint problems in order to simplify further analysis. The mechanical adjoint problem reads:

$$v \in \mathcal{V}(\mathcal{D}) \;:\; \int_{\mathcal{D}} \sigma(v) \cdot (\nabla\xi)^s = \int_{\Gamma^\star} (e + k_s v) \cdot \xi \quad \forall \xi \in \mathcal{V}(\mathcal{D}) \,. \tag{2.16}$$

The thermal adjoint problem is stated as

$$\varphi \in H^1_0(\mathcal{D}) \;:\; \int_{\mathcal{D}} q(\varphi) \cdot \nabla\eta = \int_{\mathcal{D}} \rho\beta \mathrm{div}(v)\, \eta \quad \forall \eta \in H^1_0(\mathcal{D}) \,, \tag{2.17}$$

where v and φ denote the adjoint displacement and temperature.

3. Topology optimization problem formulation

In order to design thermo-mechanical devices, the shape functional $\mathcal{J}(u)$ was proposed in eq. (2.1). The objective is to maximize the displacement u over $\Gamma^\star$ in the direction e. Therefore, to obtain the topological sensitivity of the problem under consideration it is necessary to define two classes of topological perturbations: (i) in the mechanical state, and (ii) in the thermal state. Both cases are completely independent.

3.1. **Topological perturbation in the structural part.**

For this case of perturbations, the disc $\mathcal{B}_\varepsilon$ is introduced at $\widehat{x} \in \mathcal{D}$ with constitutive properties characterized by a contrast parameters γ given by (1.11).

By considering the definition of the constitutive properties and contrast parameters presented in (1.11) (see Fig. 6), the following theorem can be stated:

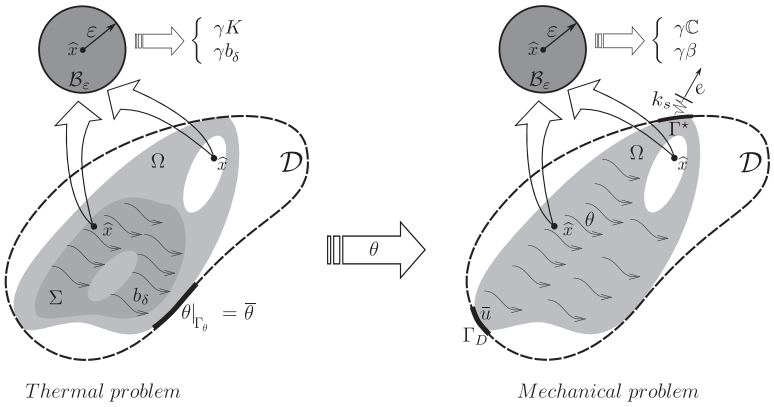

FIGURE 6. Topological perturbation in the structural part.

Theorem 3.1. *The topological derivative of the shape functional* (2.1)*, for a topological perturbation characterized by the contrast parameters* (1.11) *is given by:*

$$\mathcal{T}_\chi(\widehat{x}) = -\mathbb{P}_\gamma\sigma(u)(\widehat{x})\cdot(\nabla p)^s(\widehat{x}) + \rho\beta(1+\alpha_1)\frac{1-\gamma}{1+\gamma\alpha_1}\theta(\widehat{x})\mathrm{div}(v)(\widehat{x}) - \mathrm{P}_\gamma q(\theta)(\widehat{x})\cdot\nabla\varphi(\widehat{x}) - (1-\gamma)b_\delta\varphi(\widehat{x})\,. \tag{3.1}$$

where the fourth- and second- order polarization tensors respectively denoted by $\mathbb{P}_\gamma$ *and* P_γ*, are defined as:*

$$\mathbb{P}_\gamma = \frac{1-\gamma}{1+\gamma\alpha_2}\left((1+\alpha_2)\mathbb{I} + \frac{1}{2}(\alpha_1-\alpha_2)\frac{1-\gamma}{1+\gamma\alpha_1}\mathrm{I}\otimes\mathrm{I}\right)\,, \tag{3.2}$$

$$\mathrm{P}_\gamma = 2\frac{1-\gamma}{1+\gamma}\mathrm{I}\,. \tag{3.3}$$

since the constants α_1 *and* α_2 *are:*

$$\alpha_1 = \frac{\mu+\lambda}{\mu} \quad \textit{and} \quad \alpha_2 = \frac{3\mu+\lambda}{\mu+\lambda}\,. \tag{3.4}$$

Proof is given in Appendix.

3.2. **Topological perturbation in the heat source.** The aim of this case is to design the support of the heat sources acting in the structural part of the device Ω. To this end, the disc $\mathcal{B}_\varepsilon$ is introduced at $\widehat{x}\in\Omega$, with a heat source characterized by the contrast parameter γ^b, see Fig. 7. Therefore, the heat source for the perturbed configuration for problem (2.11) is given by (1.11).

When a topological perturbation is only considered in the heat source, see (1.11), the following theorem can be written:

Theorem 3.2. *The topological derivative of the shape functional* (2.1)*, for a topological perturbation characterized by the contrast parameter* (1.11) *is given by:*

$$\mathcal{T}_{\chi_b}(\widehat{x}) = -(1-\gamma^b)b_\delta\varphi(\widehat{x})\,. \tag{3.5}$$

Proof is given in the Appendix.

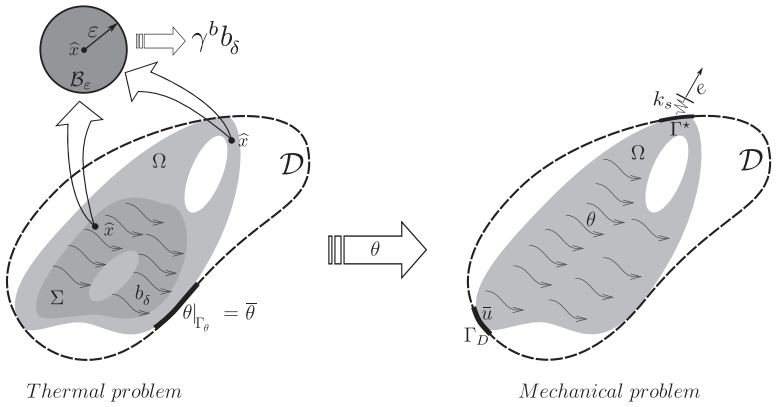

FIGURE 7. Topological perturbation in the heat source.

3.3. **Topology optimization procedure.** The optimization procedure is based on representing the structural domain and the support of the heat source in a bi-material fashion. The material distribution in $\mathcal{D}$, Ω and Σ will be identified by the characteristics functions χ and χ_b. The inclusions of weak (or less conductive) material ($\gamma < 1$) are used to mimic the holes. Based on this approach, the properties of the domains $\mathcal{D}$, Ω and Σ, and its characteristics functions χ and χ_b, are correlated with the contrast parameters γ and γ^b (see Figure 8). Note that the heat source only can be applied on the structural part of the device ($\Sigma \subseteq \Omega$). This condition can be written as $\text{Supp}(\chi_b) \subseteq \text{Supp}(\chi)$.

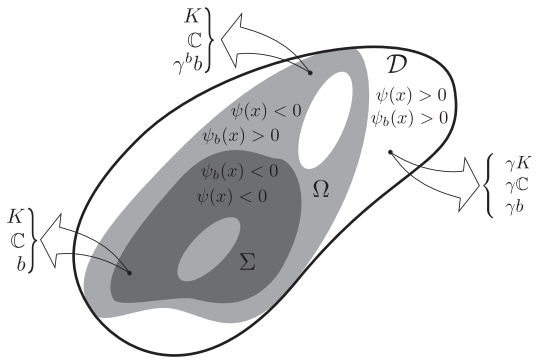

FIGURE 8. Bi-material distribution in the domains $\mathcal{D}$, Ω and Σ.

A general optimization problem with a volume constraint on the structural part can be stated as: Find the domains $\Omega \in \mathcal{D}$ and $\Sigma \in \Omega$ (characterized by the functions χ and χ_b, respectively) such that,

$$\left\{ \begin{array}{lll} \underset{\chi,\chi_b}{\text{Minimize}} & \Psi(\chi,\chi_b) & := \mathcal{J}(u), \\ \text{Subjected to} & c(\chi) := \int_{\mathcal{D}} (\chi - V^*) dx & = 0, \end{array} \right. \tag{3.6}$$

where V^* is the required volume of the structural part at the end of the optimization process.

An efficient approach to solve problem (3.6) is the use of the method proposed in [2]. The procedure relies on the level-set domain representation [19] and the approximation of the topological optimality conditions by a fixed point iteration. The topological derivative is used as a feasible descent direction to minimize the cost function $\mathcal{J}(u)$. For completeness, in the following, some remarks about the algorithm are detailed. For further details we refer to the work in [2, 3, 15].

- The definition of the domains lies on the level set functions ψ and ψ_b. The design variables are no longer the characteristics functions χ and χ_b. In fact, they are parametrized by the level-set ψ and ψ_b as

$$\chi(x) = \begin{cases} 1 & \text{if} \quad \psi(x) < 0, \\ 0 & \text{if} \quad \psi(x) > 0, \end{cases} \qquad \text{and} \quad \chi_b(x) = \begin{cases} 1 & \text{if} \quad \psi_b(x) < 0, \\ 0 & \text{if} \quad \psi_b(x) > 0. \end{cases} \tag{3.7}$$

- In order to satisfy the constraint $c(\chi) = 0$ an augmented Lagrangian method is used, as in [4, 15]. Thereby, a Lagrange multiplier λ appears as a new unknown, and a penalty parameter ρ must be provided. The optimization problem (3.6) becomes the following saddle point problem,

$$\underset{\lambda}{\text{Maximize}} \quad \underset{\chi,\chi_b}{\text{Minimize}} \quad \Psi(\psi,\psi_b) + \lambda c(\psi) + \frac{1}{2}\rho c(\psi)^2 \,. \tag{3.8}$$

- An extended topological derivatives are defined as,

$$g(x) := \begin{cases} -\mathcal{T}_\chi(x) - \max(0, \lambda + \rho c(\psi)) & \text{if} \quad \psi(x) < 0, \\ \mathcal{T}_\chi(x) + \max(0, \lambda + \rho c(\psi)) & \text{if} \quad \psi(x) > 0. \end{cases} \tag{3.9}$$

$$g_b(x) := \begin{cases} -\mathcal{T}_{\chi_b}(x) & \text{if} \quad \psi_b(x) < 0, \\ \mathcal{T}_{\chi_b}(x) & \text{if} \quad \psi_b(x) > 0. \end{cases} \tag{3.10}$$

- The optimality condition, see [2], is based on seeking $\psi(x)$ parallel to $g(x)$ and $\psi_b(x)$ parallel to $g_b(x)$. Thus, sharp interpolation schemes are used. These schemes can be written for an iteration $n+1$ as

$$\psi^{n+1} = \frac{1}{\sin\theta^n}[\sin((1-\kappa^n)\theta^n)\psi^n + \sin(\kappa^n\theta^n)\frac{g^n}{||g^n||_{L^2}}], \tag{3.11}$$

$$\psi_b^{n+1} = \frac{1}{\sin\theta_b^n}[\sin((1-\kappa_b^n)\theta_b^n)\psi_b^n + \sin(\kappa_b^n\theta_b^n)\frac{g_b^n}{||g_b^n||_{L^2}}], \tag{3.12}$$

where $\kappa^n \in [0,1]$ and $\kappa_b^n \in [0,1]$ are a step size determined by a line-search in order to decrease the value of the cost functional $\Psi(\chi,\chi_b)$. To find κ^n the level-set function ψ_b is kept fixed. On the other hand, to find κ_b^n the level-set function ψ^n is considered. The convergence criteria are based on the values of θ^n and θ_b^n, the angles between (ψ^n, g^n) and (ψ_b^n, g_b^n) , respectively, which are obtained as

$$\theta^n = \operatorname{acos}\left[\frac{\langle\psi^n, g^n\rangle}{||\psi^n||_{L^2}||g^n||_{L^2}}\right] \quad \text{and} \quad \theta_b^n = \operatorname{acos}\left[\frac{\langle\psi_b^n, g_b^n\rangle}{||\psi_b^n||_{L^2}||g_b^n||_{L^2}}\right]. \tag{3.13}$$

Note that, in this fixed point scheme, the topological derivative plays the role of the gradient in the steepest descent algorithm. Regarding to numerical aspects, a standard FEM is used for solving problems (2.2), (2.11), (2.16) and (2.17). Based

on the above description, the main steps of the algorithm can be summarized as following:

(1) Choose an initial level-set functions (ψ^0 and ψ_b^0, with $\text{Supp}(\psi_b^0) \subseteq \text{Supp}(\psi^0)$) by defining the initial guesses for the design domains;
(2) Define the characteristic functions χ and χ_b according to (3.7);
(3) Define the constitutive properties and the heat source for the finite elements in each domain associated with χ and χ_b according to (1.11) (see Fig. 8);
(4) Obtain the discretized fields u, θ, v and φ by solving, respectively, the problems (2.2), (2.11), (2.16) and (2.17);
(5) Compute the topological derivative fields $\mathcal{T}_\chi$ and $\mathcal{T}_{\chi_b}$ from eqs. (3.1) and (3.5) at Gauss point of the finite element and perform a standard nodal averaging procedure;
(6) Obtain the functions $g(x)$ and $g_b(x)$ according to (3.9) and (3.10) by using the nodal values of the topological derivatives and compute the θ and θ_b angles with (3.13);
(7) Update the level-set function ψ^{n+1} according to (3.11) and update the characteristic functions χ and χ_b according to (3.7);
(8) Check convergence $\theta^{n+1} \leq \epsilon_\theta$ where ϵ_θ is a pre-specified convergence tolerance. If True: Next. If False: goto 3.
(9) Compute functional $\Psi(\psi^{n+1}, \psi_b^n)$.
(10) Update the level-set function ψ_b^{n+1} according to (3.12) and update the characteristic functions χ_b according to (3.7);
(11) Check convergence $\theta_b^{n+1} \leq \epsilon_\theta$. If True: Next. If False: goto 3.
(12) Compute functional $\Psi(\psi^n, \psi_b^{n+1})$.
(13) Select the pair of level-set functions (ψ^{n+1}, ψ_b^n) for Ψ^{n+1} if $\Psi(\psi^{n+1}, \psi_b^n) \leq \Psi(\psi^n, \psi_b^{n+1})$. Otherwise, select the pair (ψ^n, ψ_b^{n+1}).

4. Representative numerical simulations

To illustrate the applicability of expression for the topological derivatives $\mathcal{T}_\chi$, $\mathcal{T}_{\chi_b}$ and the optimization procedure presented in the previous Section, two numerical examples are presented. All them are solved under 2D elastic plane stress assumptions. In all examples we consider the following constitutive properties: $E = 1\,\text{GPa}$ (Young's modulus), $\nu = 0.3$ (Poisson's ratio), $\alpha = 1.0 \times 10^{-6}\,\text{K}^{-1}$ and $k = 1.0\,\text{W/mK}$. The contrast parameters are given by $\rho_0 = 1.0 \times 10^{-4}$, which are used to mimic the voids, and $\delta_0 = 1.0 \times 10^{-7}$. In the part of the free boundary where nothing is specified, we consider homogeneous Neumann boundary conditions in both problems (mechanical and thermal). The direction e is given by a unit vector on $\Gamma^\star$. The thermo-mechanical problem (2.2), the steady-state heat conduction problem (2.11) and the adjoint equations (2.16) and (2.17) are solved by using the standard finite element method. The initial mesh is generated from a regular grid of size 20×12 square elements, where each resulting square is divided into four triangles, leading to 960 elements. Then, four steps of uniform mesh refinement are performed during the iterative process. In the figures, black and white are respectively used to represent solid and void faces in the structural part and the existence (or not) of the heat source in the thermal problem.

4.1. **Example 1: Amplifier.** The first example is the optimization of a displacement amplifier. This device is used to amplify the displacements in a given direction generated by thermal effects. In particular, the design domain considered is presented in Fig. 9, in which only one quadrant of the complete domain is represented, based on horizontal and vertical symmetry assumptions (the dashed-dot lines indicate the axes of symmetry). The objective is the maximization of the outward output displacement in the direction e on $\Gamma^\star$ in response to a thermal excitation imposed on Γ_θ. In this case, the boundary condition is given by a linear temperature distribution on Γ_θ, as shown in Fig. 9(b). The material properties are optimized in white subdomains, while in the light grey regions of Figs. 9(a) and 9(b) the material properties are fixed. For this example, the desired volume fractions of the structural part were fixed in 30%, 40% and 60% of the initial domain.

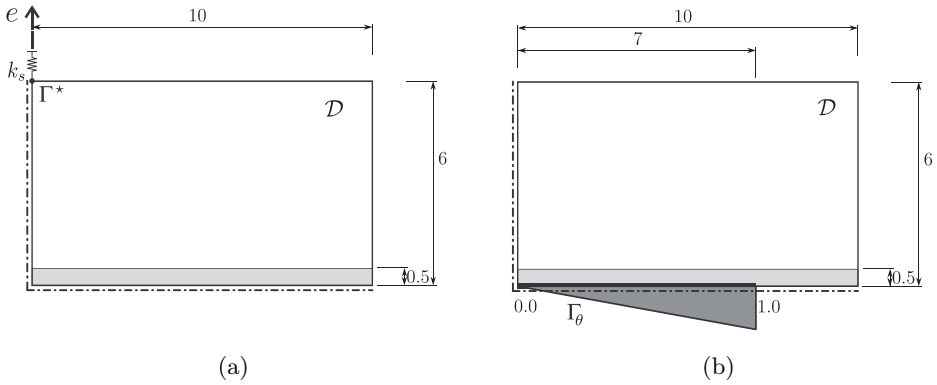

FIGURE 9. Example 1. Domain and boundary conditions: (a) mechanical problem and (b) heat problem (dimensions in mm).

In Figs. 10 to 13 the obtained results for 30% of volume fraction are shown. In order to analyze the results from a quantitative point of view we define an effectiveness factor $\Lambda := \mathcal{J}_\Omega(u_{opt})/\mathcal{J}_\Omega(u_{ini})$, where u_{ini} and u_{opt} are the displacements of the *initial* and *optimized* configurations, respectively. The behavior of effectiveness factor Λ with respect to the spring stiffness k_s for different values of the thermal source b_δ is presented in Fig. 14. Note that the highest value of Λ is achieved for the lowest value of k_s independently of the thermal source magnitude, the volume fraction and the topology. A physical explanation of this behaviour can be drawn by considering that when the spring stiffness k_s decrease, the amplifier in this point is free to move in the desired direction. The influence of the thermal source is negligible for high values of the spring stiffness k_s. This behaviour can be explained due to the high spring stiffness, in fact the spring generate a resistance to the movement in this point that cannot be compensated by the expansion introduced by thermal source.

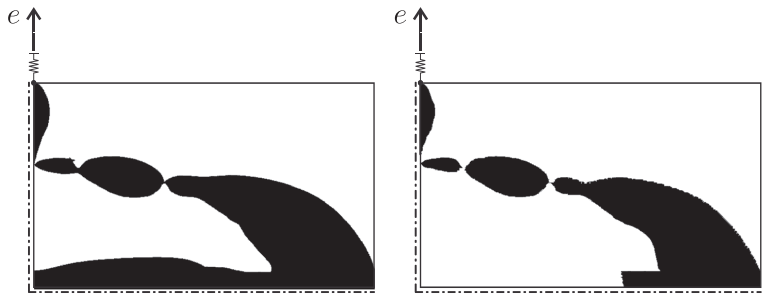

(a) structural part (b) heat source

FIGURE 10. Example 1. Obtained topologies for 30% of volume fraction, $k_s = 1 \times 10^{-4}$ [kN/mm] and $b_\delta = 1 \times 10^{-6}$. Structural response $\eta = 5 \times 10^{-6}$.

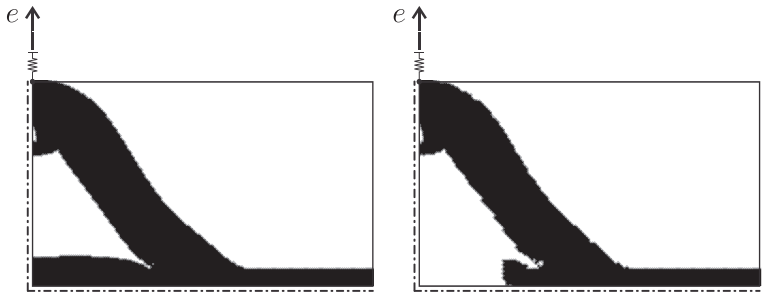

(a) structural part (b) heat source

FIGURE 11. Example 1. Obtained topologies for 30% of volume fraction, $k_s = 1 \times 10^{4}$ [kN/mm] and $b_\delta = 1 \times 10^{-6}$. Structural response $\eta = 5 \times 10^{2}$.

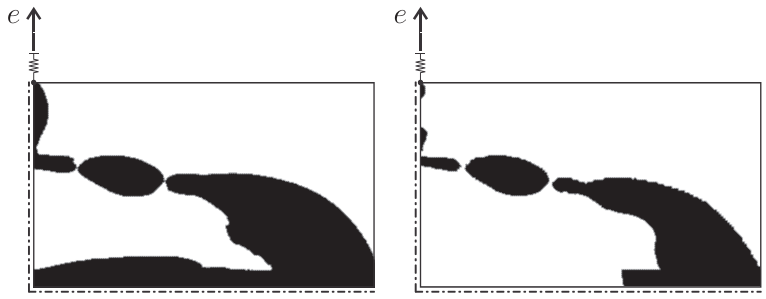

(a) structural part (b) heat source

FIGURE 12. Example 1. Obtained topologies for 30% of volume fraction, $k_s = 1 \times 10^{-4}$ [kN/mm] and $b_\delta = 1 \times 10^{-3}$. Structural response $\eta = 5 \times 10^{-6}$.

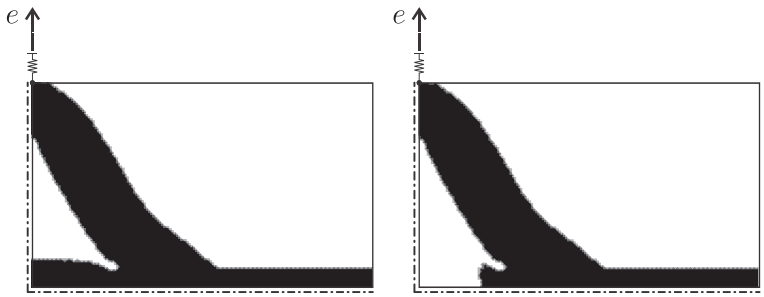

(a) structural part (b) heat source

FIGURE 13. Example 1. Obtained topologies for 30% of volume fraction, $k_s = 1 \times 10^4$ [kN/mm] and $b_\delta = 1 \times 10^{-3}$. Structural response $\eta = 5 \times 10^2$.

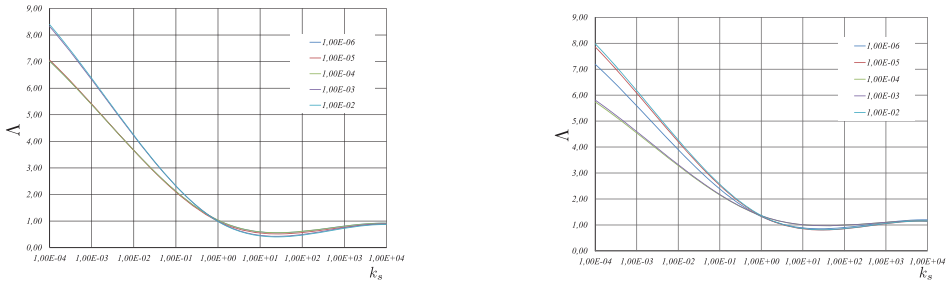

(a) 30% of volume fraction (b) 60% of volume fraction

FIGURE 14. Example 1. Comparison of Λ vs. k_s [kN/mm], for different values of thermal source b_δ.

Note that from the results presented previously, when the parameter η tends to zero the main component of the optimal topology tend to a horizontal bar, see Figs. 10 and 12. On the contrary, when η increase the main component tend to a vertical bar, see Figs. 11 and 13. These conclusions are similar to the presented in the motivational example in Section 1.1 and confirm the fundamental aspect of the structural response parameter η.

4.2. **Example 2: Inverter.** The second example considers the same domain from the previous experiment, however, the output displacement region $\Gamma^\star$ is changed as depicted in Fig. 15. This apparently simple modification in the design domain actually results in a completely different mechanism, since the optimizer seeks an output displacement contrary to the natural movement of the thermo-mechanical device. In addition, all symmetry assumptions remain valid and the boundary condition for thermal problem is given by a linear temperature distribution on Γ_θ, as shown in Fig. 15(b). The material properties are optimized in white subdomains, while in the light grey regions of Figs. 15(a) and 15(b) the material properties are fixed, as in the previous example.

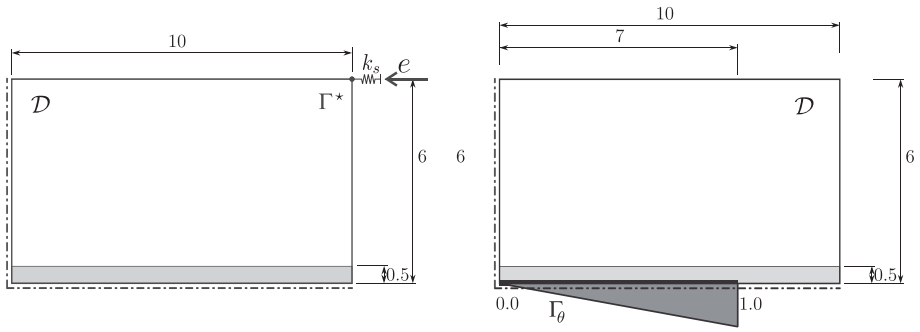

(a) (b)

FIGURE 15. Example 2. Domain and boundary conditions: (a) mechanical problem and (b) heat problem (dimensions in mm).

The obtained results for 40% and 60% of volume fraction are shown in Figs. 16 and 17, for a selected values of k_s and b_δ. The variation in the values for the effectiveness factor Λ with respect to the spring stiffness k_s and the thermal source b for the obtained results are presented in Fig. 18. Note that the negative sign for Λ indicates the inversion of the direction of the displacement. As analysed in the previous example, the lowest value of Λ is achieved for the lowest value of k_s, independently of the thermal source magnitude, the volume fraction and the final topology. Also, the influence of the thermal source value in Λ decreases for high values of the spring stiffness k_s.

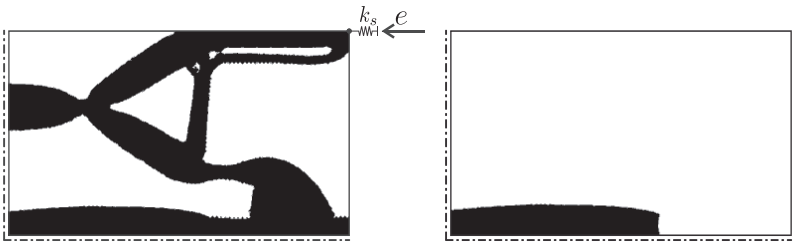

(a) structural part (b) heat source

FIGURE 16. Example 2. Obtained topologies for 40% of volume fraction, $k_s = 1$ [kN/mm] and $b_\delta = 1$. Structural response $\eta = 5 \times 10^{-2}$.

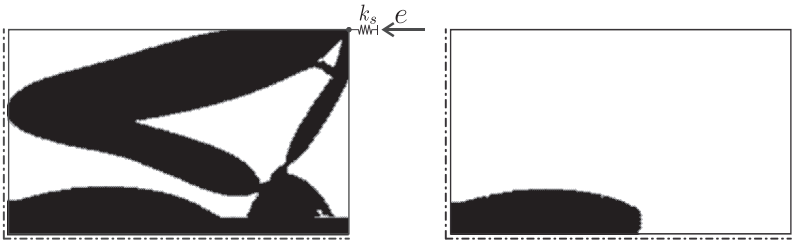

(a) structural part (b) heat source

FIGURE 17. Example 2. Obtained topologies for 60% of volume fraction, $k_s = 1$ [kN/mm] and $b_\delta = 1$. Structural response $\eta = 5 \times 10^{-2}$.

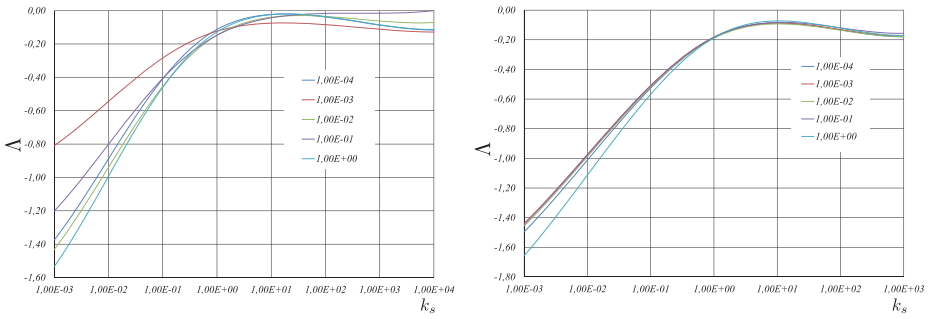

(a) 40% of volume fraction (b) 60% of volume fraction

FIGURE 18. Example 2. Comparison Λ vs. k_s [kN/mm], for different values of thermal source b_δ.

5. Concluding remarks

In the paper a methodology for the optimal design of a thermo-mechanical device are presented. For the optimal design procedure was considered as unknown the topology of the structural part of the device and the support of the applied thermal source. For this case, the topological derivative of the tracking-type shape functional for the coupled models of thermo-mechanical type are derived in two spatial dimensions. By introducing contrasts on the thermal conductivity coefficient, the elastic modulus and the thermal source, an simple and analytical expressions of the topological derivatives were obtained to be used in the topological design of thermal-mechanical actuators. The information provided by $\mathcal{T}_\chi(\hat{x})$ and $\mathcal{T}_{\chi_b}(\hat{x})$ can be used as a steepest descent direction in an optimal design algorithm. To illustrate this feature, two numerical experiment associated to the topology optimization of actuators have been presented. These simples examples show the applicability of the proposed methodology in the context of optimal design of thermal-mechanical devices. Furthermore, we shown that the proposed methodology is able to design the region where the heat source must be applied in order to maximize the efficiency of the actuator. Also, a qualitative study of the influence of the spring stiffness in

the optimal design and it's efficiency was carried out. From this study, can be concluded that the efficiency of the actuator decreases for high values of the spring stiffness independently of the heat source value, final volume fraction and topology.

Acknowledgments

This research was partly supported by the Argentinean Research and Development Program of the National Technological University (PID-UTN), Argentinean National Council for Scientific and Technical Research (CONICET), Argentinean National Agency for Scientific and Technical Promotion (ANPCyT), and by the Brazilian Research Council (CNPq). The support of these agencies is gratefully acknowledged. J.S. acknowledges the support of the French Agence Nationale de la Recherche (ANR), under grant ANR-17-CE08-0039 (project ArchiMatHOS).

Appendix A. Existence of the topological derivative

In order to prove the Theorems 3.1 and 3.2 we need technical results which are given with proofs.

We recall that the scalar function θ_ε solves the following perturbed variational problem: Find the temperature field $\theta_\varepsilon \in \mathcal{H}(\Omega)$, such that

$$\int_\Omega q_\varepsilon(\theta_\varepsilon)\cdot\nabla\eta + \int_\Omega b_\varepsilon\eta = 0 \quad \forall \eta \in \mathcal{H}_0(\Omega), \tag{A.1}$$

where

$$q_\varepsilon(\theta_\varepsilon) := -\gamma_\varepsilon^T \mathrm{K}\nabla\theta_\varepsilon, \quad b_\varepsilon := \gamma_\varepsilon^T b_\delta, \tag{A.2}$$

with the contrast on the thermal properties defined as

$$\gamma_\varepsilon^T := \begin{cases} 1 & \text{in} \quad \Omega \setminus \overline{B_\varepsilon} \\ \gamma^T & \text{in} \quad B_\varepsilon \end{cases} . \tag{A.3}$$

Proposition A.1. *Let θ and θ_ε be solutions to* (2.11) *and* (A.1)*, respectively. Then we have that the following estimate holds true*

$$\|\theta_\varepsilon - \theta\|_{H^1(\Omega)} \leq C\varepsilon. \tag{A.4}$$

Proof. We start by subtracting the variational problem (2.11) from (A.1). After some manipulations there is:

$$\int_\Omega q_\varepsilon(\theta_\varepsilon - \theta)\cdot\nabla\eta = (1-\gamma^T)\int_{B_\varepsilon} q(\theta)\cdot\nabla\eta + (1-\gamma^T)\int_{B_\varepsilon} b_\delta\eta, \tag{A.5}$$

where we have used the fact that $q_\varepsilon(\phi) = q(\phi)$ and $b_\varepsilon = b_\delta$ in $\Omega \setminus \overline{B_\varepsilon}$, and $q_\varepsilon(\phi) = \gamma^T q(\phi)$ and $b_\varepsilon = \gamma^T b_\delta$ in B_ε. By taking $\eta = \theta_\varepsilon - \theta$ as a test function in the above equation we obtain the following equality

$$\int_\Omega q_\varepsilon(\theta_\varepsilon-\theta)\cdot\nabla(\theta_\varepsilon-\theta) = (1-\gamma^T)\int_{B_\varepsilon} q(\theta)\cdot\nabla(\theta_\varepsilon-\theta) + (1-\gamma^T)\int_{B_\varepsilon} b_\delta(\theta_\varepsilon-\theta). \tag{A.6}$$

From the Cauchy-Schwartz inequality it follows that

$$\begin{aligned}\int_\Omega q_\varepsilon(\theta_\varepsilon-\theta)\cdot\nabla(\theta_\varepsilon-\theta) &\le C_1\|q(\theta)\|_{L^2(B_\varepsilon)}\|\nabla(\theta_\varepsilon-\theta)\|_{L^2(B_\varepsilon)}\\ &\quad + C_2\|b\|_{L^2(B_\varepsilon)}\|\theta_\varepsilon-\theta\|_{L^2(B_\varepsilon)}\\ &\le \varepsilon C_3\|\theta_\varepsilon-\theta\|_{H^1(\Omega)},\end{aligned} \tag{A.7}$$

where we have used the interior elliptic regularity of function θ and the continuity of the function b at the point $\widehat{x}\in\Omega$. Finally, from the coercivity of the bilinear form on the left-hand side of (A.5), namely

$$c\|\theta_\varepsilon-\theta\|^2_{H^1(\Omega)} \le \int_\Omega q_\varepsilon(\theta_\varepsilon-\theta)\cdot\nabla(\theta_\varepsilon-\theta), \tag{A.8}$$

we obtain the result with the constant $C=C_3/c$ independent of the small parameter ε. □

The vector function u_ε is the solution to the perturbed coupled system, namely: Find the displacement field $u_\varepsilon\in\mathcal{V}(\Omega)$, such that

$$\int_\Omega \sigma_\varepsilon(u_\varepsilon)\cdot(\nabla v)^s = \int_\Omega \beta_\varepsilon\theta_\varepsilon \mathrm{div}(v) \quad \forall v\in\mathcal{V}(\Omega), \tag{A.9}$$

where

$$\sigma_\varepsilon(u_\varepsilon) := \gamma^M_\varepsilon \mathbb{C}(\nabla u_\varepsilon)^s = \gamma^M_\varepsilon\sigma(u_\varepsilon), \tag{A.10}$$

with the contrast on the elastic properties defined as

$$\gamma^M_\varepsilon := \left\{\begin{array}{ccc} 1 & \text{in} & \Omega\setminus\overline{B_\varepsilon} \\ \gamma^M & \text{in} & B_\varepsilon \end{array}\right. . \tag{A.11}$$

Proposition A.2. *Let u and u_ε be solutions to* (2.2) *and* (A.9)*, respectively. Then we have that the following estimate holds true*

$$\|u_\varepsilon-u\|_{\mathbf{H}^1(\Omega)} \le C\varepsilon. \tag{A.12}$$

Proof. Let us subtract the variational problem (2.2) from (A.9), so that after some manipulations we have:

$$\begin{aligned}\int_\Omega \sigma_\varepsilon(u_\varepsilon-u)\cdot(\nabla v)^s &= \int_\Omega \beta(\theta_\varepsilon-\theta)\mathrm{div}(v) + (1-\gamma^M)\\ &\quad \int_{B_\varepsilon}(\sigma(u)+\beta\theta\,\mathrm{I})\cdot(\nabla v)^s - (1-\gamma^M)\\ &\quad \int_{B_\varepsilon}\beta(\theta_\varepsilon-\theta)\mathrm{div}(v),\end{aligned} \tag{A.13}$$

where we have used the fact that $\sigma_\varepsilon(\phi)=\sigma(\phi)$ and $\beta_\varepsilon=\beta$ in $\Omega\setminus\overline{B_\varepsilon}$, and $\sigma_\varepsilon(\phi)=\gamma^M\sigma(\phi)$ and $\beta_\varepsilon=\gamma^M\beta$ in B_ε. By taking $v=u_\varepsilon-u$ as test function in the above

equation we obtain the following equality

$$\begin{aligned}\int_\Omega \sigma_\varepsilon(u_\varepsilon - u)\cdot(\nabla(u_\varepsilon - u))^s = &\int_\Omega \beta(\theta_\varepsilon - \theta)\mathrm{div}(u_\varepsilon - u) + (1-\gamma^M)\\ &\int_{B_\varepsilon}(\sigma(u) + \beta\theta\,\mathrm{I})\cdot(\nabla(u_\varepsilon - u))^s - (1-\gamma^M)\\ &\int_{B_\varepsilon}\beta(\theta_\varepsilon - \theta)\mathrm{div}(u_\varepsilon - u).\end{aligned} \tag{A.14}$$

From the Cauchy-Schwartz inequality it follows that

$$\begin{aligned}\int_\Omega \sigma_\varepsilon(u_\varepsilon - u)\cdot(\nabla(u_\varepsilon - u))^s &\le C_1\|\theta_\varepsilon - \theta\|_{L^2(\Omega)}\|\nabla(u_\varepsilon - u)\|_{\mathbf{L}^2(\Omega)}\\ &\quad + C_2\|\sigma(u) + \beta\theta\,\mathrm{I}\|_{\mathbf{L}^2(B_\varepsilon)}\|\nabla(u_\varepsilon - u)\|_{\mathbf{L}^2(B_\varepsilon)}\\ &\quad + C_3\|\theta_\varepsilon - \theta\|_{L^2(B_\varepsilon)}\|\nabla(u_\varepsilon - u)\|_{\mathbf{L}^2(B_\varepsilon)}\\ &\le C_4\|\theta_\varepsilon - \theta\|_{H^1(\Omega)}\|u_\varepsilon - u\|_{\mathbf{H}^1(\Omega)}\\ &\quad + \varepsilon C_5\|u_\varepsilon - u\|_{\mathbf{H}^1(\Omega)},\end{aligned} \tag{A.15}$$

where we have used the interior elliptic regularity of function u and the continuity of the function β at the point $\widehat{x} \in \Omega$. From Lemma A.1 we have now

$$\int_\Omega \sigma_\varepsilon(u_\varepsilon - u)\cdot(\nabla(u_\varepsilon - u))^s \le C_6\varepsilon\|u_\varepsilon - u\|_{\mathbf{H}^1(\Omega)}. \tag{A.16}$$

Finally, from the coercivity of the bilinear form on the left-hand side of (A.13), namely

$$c\|u_\varepsilon - u\|^2_{\mathbf{H}^1(\Omega)} \le \int_\Omega \sigma_\varepsilon(u_\varepsilon - u)\cdot(\nabla(u_\varepsilon - u))^s, \tag{A.17}$$

we obtain the result with the constant $C = C_6/c$ independent of the small parameter ε. □

Finally, the topologically perturbed counterpart of the mechanical adjoint problem (2.16) reads: Find the adjoint displacement field $p_\varepsilon \in \mathcal{V}(\Omega)$, such that

$$\int_\Omega \sigma_\varepsilon(p_\varepsilon)\cdot(\nabla v)^s = \int_{\Gamma^\star} e\cdot v \quad \forall v \in \mathcal{V}(\Omega), \tag{A.18}$$

while the topologically perturbed counterpart of the thermal adjoint problem (2.17) is given by: Find the adjoint temperature field $\varphi_\varepsilon \in \mathcal{H}_0(\Omega)$, such that

$$\int_\Omega q_\varepsilon(\varphi_\varepsilon)\cdot\nabla\eta = \int_\Omega \beta\mathrm{div}(p)\,\eta \quad \forall \eta \in \mathcal{H}_0(\Omega). \tag{A.19}$$

Proposition A.3. *Let p and p_ε be solutions to* (2.16) *and* (A.18)*, respectively. Then we have that the following estimate holds true*

$$\|p_\varepsilon - p\|_{\mathbf{H}^1(\Omega)} \le C\varepsilon. \tag{A.20}$$

Proof. After subtracting the variational problem (2.16) from (A.18) we have:

$$\int_\Omega \sigma_\varepsilon(p_\varepsilon - p)\cdot(\nabla v)^s = (1-\gamma^M)\int_{B_\varepsilon}\sigma(p)\cdot(\nabla v)^s, \tag{A.21}$$

where we have used the fact that $\sigma_\varepsilon(\phi) = \sigma(\phi)$ in $\Omega \setminus \overline{B_\varepsilon}$ and $\sigma_\varepsilon(\phi) = \gamma^M \sigma(\phi)$ in B_ε. By taking $v = p_\varepsilon - p$ as test function in the above equation we obtain the following equality

$$\int_\Omega \sigma_\varepsilon(p_\varepsilon - p) \cdot (\nabla(p_\varepsilon - p))^s = (1 - \gamma^M) \int_{B_\varepsilon} \sigma(p) \cdot (\nabla(p_\varepsilon - p))^s. \tag{A.22}$$

From the Cauchy-Schwartz inequality it follows that

$$\int_\Omega \sigma_\varepsilon(p_\varepsilon - p) \cdot (\nabla(p_\varepsilon - p))^s \leq C_1 \|\sigma(p)\|_{\mathbf{L}^2(B_\varepsilon)} \|\nabla(p_\varepsilon - p)\|_{\mathbf{L}^2(B_\varepsilon)} \leq \varepsilon C_2 \|p_\varepsilon - p\|_{\mathbf{H}^1(\Omega)}, \tag{A.23}$$

where we have used the interior elliptic regularity of function p. Finally, from the coercivity of the bilinear form on the left-hand side of (A.21), namely

$$c\|p_\varepsilon - p\|^2_{\mathbf{H}^1(\Omega)} \leq \int_\Omega \sigma_\varepsilon(p_\varepsilon - p) \cdot (\nabla(p_\varepsilon - p))^s, \tag{A.24}$$

we obtain the result with the constant $C = C_2/c$ independent of the small parameter ε. □

Proposition A.4. *Let φ and φ_ε be solutions to* (2.17) *and* (A.19)*, respectively. Then we have that the following estimate holds true*

$$\|\varphi_\varepsilon - \varphi\|_{H^1(\Omega)} \leq C\varepsilon. \tag{A.25}$$

Proof. After subtracting the variational problem (2.17) from (A.19) there is:

$$\int_\Omega q_\varepsilon(\varphi_\varepsilon - \varphi) \cdot \nabla\eta = (1 - \gamma^T) \int_{B_\varepsilon} q(\varphi) \cdot \nabla\eta, \tag{A.26}$$

where we have used the fact that $q_\varepsilon(\phi) = q(\phi)$ in $\Omega \setminus \overline{B_\varepsilon}$ and $q_\varepsilon(\phi) = \gamma^T q(\phi)$ in B_ε. By taking $\eta = \varphi_\varepsilon - \varphi$ as test function in the above equation we obtain the following equality

$$\int_\Omega q_\varepsilon(\varphi_\varepsilon - \varphi) \cdot \nabla(\varphi_\varepsilon - \varphi) = (1 - \gamma^T) \int_{B_\varepsilon} q(\varphi) \cdot \nabla(\varphi_\varepsilon - \varphi). \tag{A.27}$$

From the Cauchy-Schwartz inequality it follows that

$$\int_\Omega q_\varepsilon(\varphi_\varepsilon - \varphi) \cdot \nabla(\varphi_\varepsilon - \varphi) \leq C_1 \|q(\varphi)\|_{L^2(B_\varepsilon)} \|\nabla(\varphi_\varepsilon - \varphi)\|_{L^2(B_\varepsilon)} \leq \varepsilon C_2 \|\varphi_\varepsilon - \varphi\|_{H^1(\Omega)}, \tag{A.28}$$

where we have used the interior elliptic regularity of function φ. Finally, from the coercivity of the bilinear form on the left-hand side of (A.26), namely

$$c\|\varphi_\varepsilon - \varphi\|^2_{H^1(\Omega)} \leq \int_\Omega q_\varepsilon(\varphi_\varepsilon - \varphi) \cdot \nabla(\varphi_\varepsilon - \varphi), \tag{A.29}$$

we obtain the result with the constant $C = C_2/c$ independent of the small parameter ε. □

Appendix B. Proof of Theorem 3.1

The reader interested in a complete development of the proof of this result may refer to [6]. For completeness, the main ingredients of the calculation of the topological derivative $\mathcal{T}_\chi(\widehat{x})$ are presented in the following. First consider the variation of the shape-functional (2.1) when a topological perturbation is introduced in the domain, given by

$$\delta\mathcal{J}_\varepsilon(u) := -\int_{\Gamma^\star} e\cdot(u_\varepsilon - u)\,, \tag{B.1}$$

where u_ε is the solution of the perturbed counterpart of the problem (2.2). After some tedious calculation, the variation $\delta\mathcal{J}_\varepsilon(u)$ can be written as:

$$\begin{aligned}\delta\mathcal{J}_\varepsilon(u) = &-\frac{1-\gamma}{\gamma}\int_{B_\varepsilon}\rho\sigma(p_\varepsilon)\cdot(\nabla u)^s\\ &+(1-\gamma)\beta\rho\int_{B_\varepsilon}\theta\mathrm{div}(p_\varepsilon)\\ &-\frac{1-\gamma}{\gamma}\int_{B_\varepsilon}\delta q(\varphi_\varepsilon)\cdot\nabla\theta\\ &-(1-\gamma)\delta\int_{B_\varepsilon} b_\delta\varphi_\varepsilon.\end{aligned} \tag{B.2}$$

where p_ε and φ_ε are the solutions of the perturbed counterparts of the problems (2.16) and (2.17), respectively. By applying classical asymptotic analysis technics, see for instance [17], the stress and flux fields $\rho\sigma(p_\varepsilon)$ and $\delta q(\varphi_\varepsilon)$ inside the ball B_ε can be written as:

$$\rho\sigma(p_\varepsilon) = \mathbb{P}_\gamma\sigma(p)(\widehat{x}) \quad\text{and}\quad \delta q(\varphi_\varepsilon) = \mathrm{P}_\gamma q(\varphi)(\widehat{x}) \tag{B.3}$$

where the tensors $\mathbb{P}_\gamma$ and P_γ are defined in (3.2)-(3.3). Next, the above results must be introduced in the expression of $\delta\mathcal{J}_\varepsilon(u)$ and the regularity of the fields p_ε and φ_ε inside the ball B_ε will be considered. The proof is completed by integrating theses fields in B_ε, dividing the result by $\pi\varepsilon^2$ and taking the limit $\varepsilon\to 0^+$.

Appendix C. Proof of Theorem 3.2

Proof. The reader interested in a complete development of the proof of this result may refer to [6]. For completeness, the main ingredients of the calculation of the topological derivative $\mathcal{T}_{\chi_b}(\widehat{x})$ are presented in the following. First consider the variation of the shape-functional (2.1) when a topological perturbation is introduced in the domain affecting only the thermal source in problem (2.11), given by

$$\delta\mathcal{J}_\varepsilon(u) := -\int_{\Gamma^\star} e\cdot(u_\varepsilon - u)\,, \tag{C.1}$$

where u_ε is the solution of the perturbed counterpart of the problem (2.2). After some tedious calculation, the variation $\delta\mathcal{J}_\varepsilon(u)$ can be written as:

$$\delta\mathcal{J}_\varepsilon(u) = -(1-\gamma^b)\delta\int_{B_\varepsilon} b_\delta\varphi_\varepsilon. \tag{C.2}$$

where φ_ε is the solution of the perturbed counterpart of the problem (2.17). Next, the regularity of the field φ_ε inside the ball B_ε will be considered. The proof is completed by integrating this field in B_ε, dividing the result by $\pi\varepsilon^2$ and taking the limit $\varepsilon \to 0^+$. □

References

[1] G. Allaire, F. Jouve and N. Van Goethem, *Damage and fracture evolution in brittle materials by shape optimization methods*, J. Comput. Phys. **230** (2011), 5010–5044.

[2] S. Amstutz and H. Andrä, *A new algorithm for topology optimization using a level-set method*, J. Comput. Phys. 216 (2006), 573–588.

[3] S. Amstutz, A. A. Novotny and E. A. de Souza Neto, *Topological derivative-based topology optimization of structures subject to Drucker-Prager stress constraints*, Comput. Methods Appl. Mech. Engrg. **233-236** (2012), 123–136.

[4] D. E. Campeão, S. M. Giusti and A. A. Novotny *Topology design of plates consedering different volume control methods*, Engrg. Comput., 31 (2014), 826–842.

[5] G. Cardone, S.A. Nazarov and J. Sokołowski, *Asymptotic analysis, polarization matrices, and topological derivatives for piezoelectric materials with small voids*, SIAM J. Control Optim. **48** (2010), 3925–3961.

[6] S. M. Giusti, Z. Mróz, A. A. Novotny and J. Sokoł owski, *Topology design of thermomechanical actuators*, Struct. Multidiscip. Optim. **55** (2017), 1575–1587.

[7] S. M. Giusti, A. A. Novotny, and E. A. de Souza Neto, *Sensitivity of the macroscopic response of elastic microstructures to the insertion of inclusions*, Proc. Roy. Soc. Sect. A, **466** (2010), 1703–1723.

[8] S. M. Giusti, A. A. Novotny, E. A. de Souza Neto and R. A. Feijóo, *Sensitivity of the macroscopic elasticity tensor to topological microstructural changes*, J. Mech. Phys. Solids **57** (2009), 555–570.

[9] S. M. Giusti, A. A. Novotny, J. E. Muñoz Rivera and J. E. Esparta Rodriguez, *Strain energy change to the insertion of inclusions associated to a thermo-mechanical semi-coupled system*, Internat. J. Solids Struct. **50** (2013), 1303–1313.

[10] M. Hintermüller and A. Laurain, *Multiphase image segmentation and modulation recovery based on shape and topological sensitivity*, J. Math. Imaging Vision **35** (2009), 1–22.

[11] M. Hintermüller, A. Laurain and A. A. Novotny, *Second-order topological expansion for electrical impedance tomography*, Adv. Comput. Math. **36** (2012), 235–265.

[12] A. Kowalewski, I. Lasiecka and J. Sokołowski, *Sensitivity analysis of hyperbolic optimal control problems*, Comput. Optim. Appl. **52** (2012),147–179.

[13] I. Lasiecka, *Mathematical Control Theory of Coupled PDEs*, *CBMS-NSF Regional Conf. Ser. in Appl. Math.*, vol. 75, 2002.

[14] I. Lasiecka and J. Sokołowski, *Sensitivity analysis of optimal control problems for wave equations*, SIAM J. Control Optim. **29** (1991), 1128–1149.

[15] C. G. Lopes, R. B. Santos and A. A. Novotny, *Topological derivative-based topology optimization of structures subject to multiple load-cases*, Lat. Am. J. Solids and Struct. **12** (2015), 834–860.

[16] S. A. Nazarov and J. Sokołowski, *Asymptotic analysis of shape functionals*, J. Math. P. Appl. **82** (2003), 125–196.

[17] A. A. Novotny and J. Sokołowski, *Topological Derivatives in Shape Optimization*, Interaction of Mechanics and Mathematics, Springer-Verlag, Berlin, Heidelberg, 2013.

[18] A. A. Novotny, J. Sokołowski and A. Zochowski, *Applications of the Topological Derivative Method*, Studies in Systems, Decision and Control. Springer-Verlag, Berlin, Heidelberg, 2019.

[19] S. Osher and J. A. Sethian, *Front propagating with curvature dependent speed: algorithms based on Hamilton-Jacobi formulations*, J. Comput. Phys. **79** (1988), 12–49.

[20] J. Sokołowski and A. Żochowski, *On the topological derivative in shape optimization*, SIAM J. Control Optim. **37** (1999), 1251–1272.

[21] N. Van Goethem and A. A. Novotny, *Crack nucleation sensitivity analysis*, Math. Methods Appl. Sci. **33** (2010), 1978–1994.

Manuscript received February 3 2019
revised May 22 2019

S. M. Giusti
Universidad Tecnológica Nacional, Facultad Regional Córdoba UNT/FRC - CONICET, Maestro M. López esq. Cruz Roja Argentina, X5016ZAA - Córdoba, Argentina
E-mail address: sgiusti@frc.utn.edu.ar

Z. Mróz
Institute of Fundamental Technological Research, 5A Pawińskiego St., 00-049 Warsaw, Poland
E-mail address: zmroz@ippt.gov.pl

A. A. Novotny
Laboratório Nacional de Computação Científica LNCC/MCT, Av. Getúlio Vargas 333, 25651-075 Petrópolis - RJ, Brasil
E-mail address: novotny@lncc.br

J. Sokołowski
Department of Scientific Computing, Informatic Center, Federal University of Paraiba, 471 Rua dos Escoteiros s/n, Mangabeira, João Pessoa, Paraiba 58058-600, Brazil
and Systems Research Institute of the Polish Academy of Sciences, 01-447 Warszawa, ul Newelska 6, Poland
and Université de Lorraine, CNRS, INRIA, Institute Élie Cartan Nancy, UMR7502, BP 239 - 54506 Vandoeuvre Lès Nancy Cedex, France
E-mail address: Jan.Sokolowski@univ-lorraine.fr